Corrosion behavior of Fe-based amorphous/nanocrystalline composite coating: correlating the influence of porosity and amorphicity

Sapan K. Nayak[1], Anil Kumar[2], Kuntal Sarkar[3], Atanu Banerjee[4], Tapas Laha[5]

[1, 2, 5] Department of Metallurgical and Materials Engineering, IIT Kharagpur, India

[3, 4] Research and Development Division, Tata Steel, Jamshedpur, India

CMDWC 2021

1st Corrosion and Materials Degradation Web Conference

17-19 MAY 2021 | ONLINE

Organized by

MONASH University · corrosion and materials degradation, an Open Access Journal by MDPI · MDPI · materials, an Open Access Journal by MDPI · The University of Akron

INTRODUCTION

❑ Fe-based amorphous coating

- Excellent mechanical and corrosion properties
- Optimized properties → strength of amorphous structure and ductility of metallic substrate
- Can be applied to complex parts
- Inexpensiveness
- Poor plasticity → limited industrial application

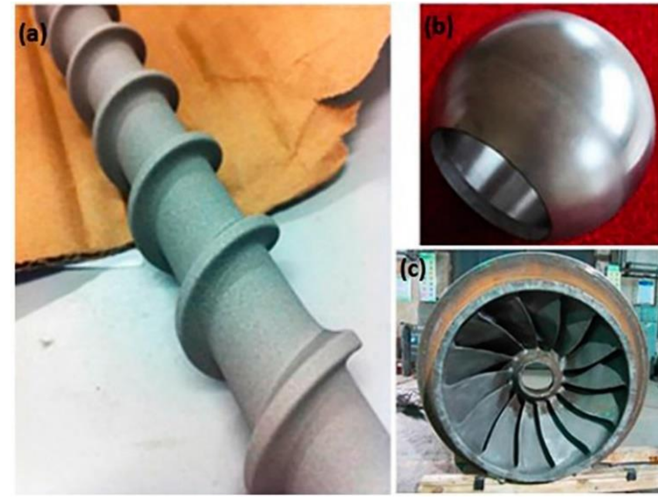

H. X. Li et al., Prog. Mat. Sci. 103 (2019) 235-318

❑ Fe-based amorphous/nanocrystalline composite coating

- No issue with poor plasticity

❑ Fe-based composite coating synthesized by thermal spraying

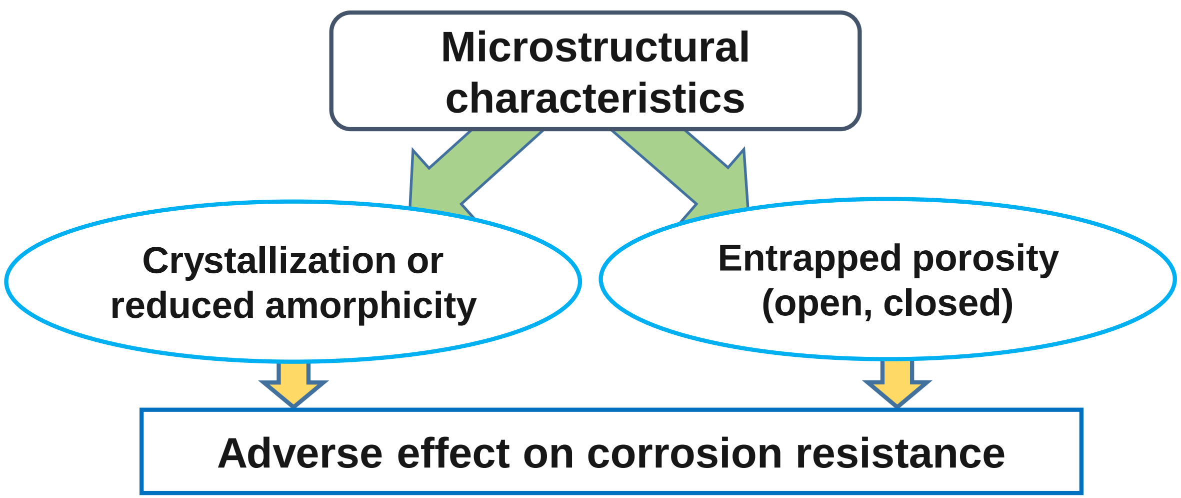

Dominant microstructural characteristic??

Help in designing new amorphous composite coatings with improved corrosion resistance.

EXPERIMENTAL PROCEDURE

I. Synthesis of the coatings and the ribbons

Spraying parameters of HVOF process for deposition of coatings

Spray parameters	Coatings	
	Coating [30 g/min]	Coating [50 g/min]
Oxygen flow rate (SLPM)	270	
Fuel gas flow rate (SLPM)	55-60	
Air flow rate (SLPM)	460	
Carrier gas flow rate (SCFH)	15-18	
Spray distance (mm)	150	
Powder feed rate (g/min)	30	50
Coating thickness (μm)	150 ± 15	

Melt-spinning parameters for ribbons

Ribbons	Wheel speed (rpm)
Fully amorphous (FA-Rib)	2100
Partially amorphous (PA-Rib)	1400

Preparation of the different coatings along with the ribbons → identifying effect of amorphous content and porosity individually on the corrosion behavior of the sprayed coatings

II. Electrochemical characterization

- Electrolyte: 3.5 wt% NaCl solution
- Potentiodynamic polarization study: scan rate of 0.5 mV/s after 1 h of immersion for stabilization of open circuit potential (OCP)
- EIS test (OCP): sinusoidal amplitude of 10 mV in the frequency range of 10^5 to 10^{-2} Hz
- Pontentiostatic test at 500 mV_{SCE}: passive film

III. Analysis of corroded samples

- Raman spectrometer (Co laser of 532 nm wavelength): compositional analysis
- Auger electron spectroscopy: depth profiling→ effective sputtering rate of 1.8 nm min^{-1}

Morphology of the synthesized ribbons and coatings

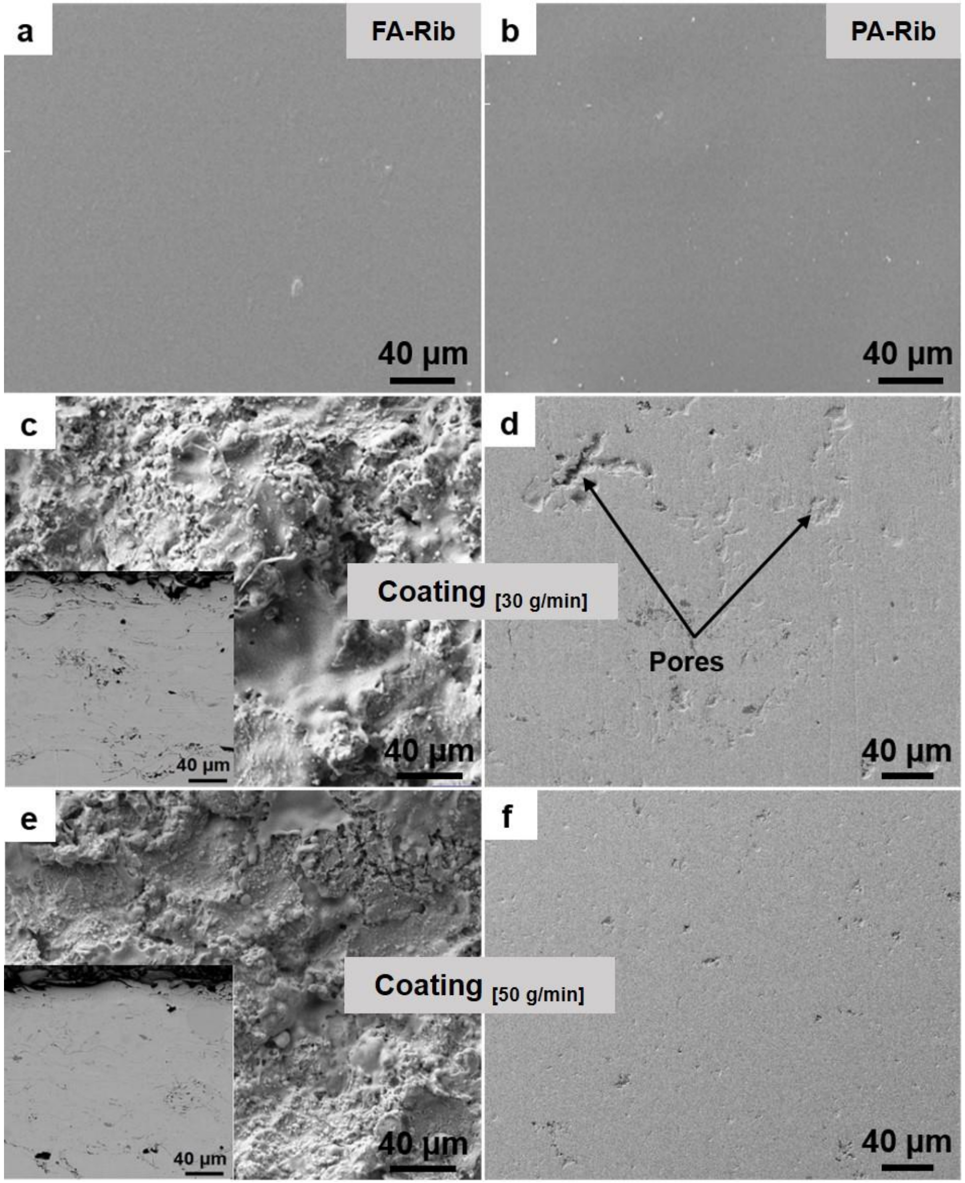

Composition: $Fe_{63}Cr_9B_{16}C_7P_5$, at. %

Sample	Porosity (vol.%)
FA-Rib	–
PA-Rib	–
Coating $_{[30\ g/min]}$	4.9 ± 0.6
Coating $_{[50\ g/min]}$	1.8 ± 0.4

- **Ribbons → porosity free structure**
- **Coating $_{[30\ g/min]}$ → greater extent of molten particles and inferior inter-splat bonding and higher amount of porosity than that of Coating $_{[50\ g/min]}$**

SEM images of the ribbons: (a) FA-Rib, (b) PA-Rib, and the coatings: (c–d) Coating $_{[30\ g/min]}$ and (e–f) Coating $_{[50\ g/min]}$

S.K. Nayak et al., J. Alloys Compd. 849 (2020) 156624

RESULTS

Phase evolution in the ribbons and the coatings

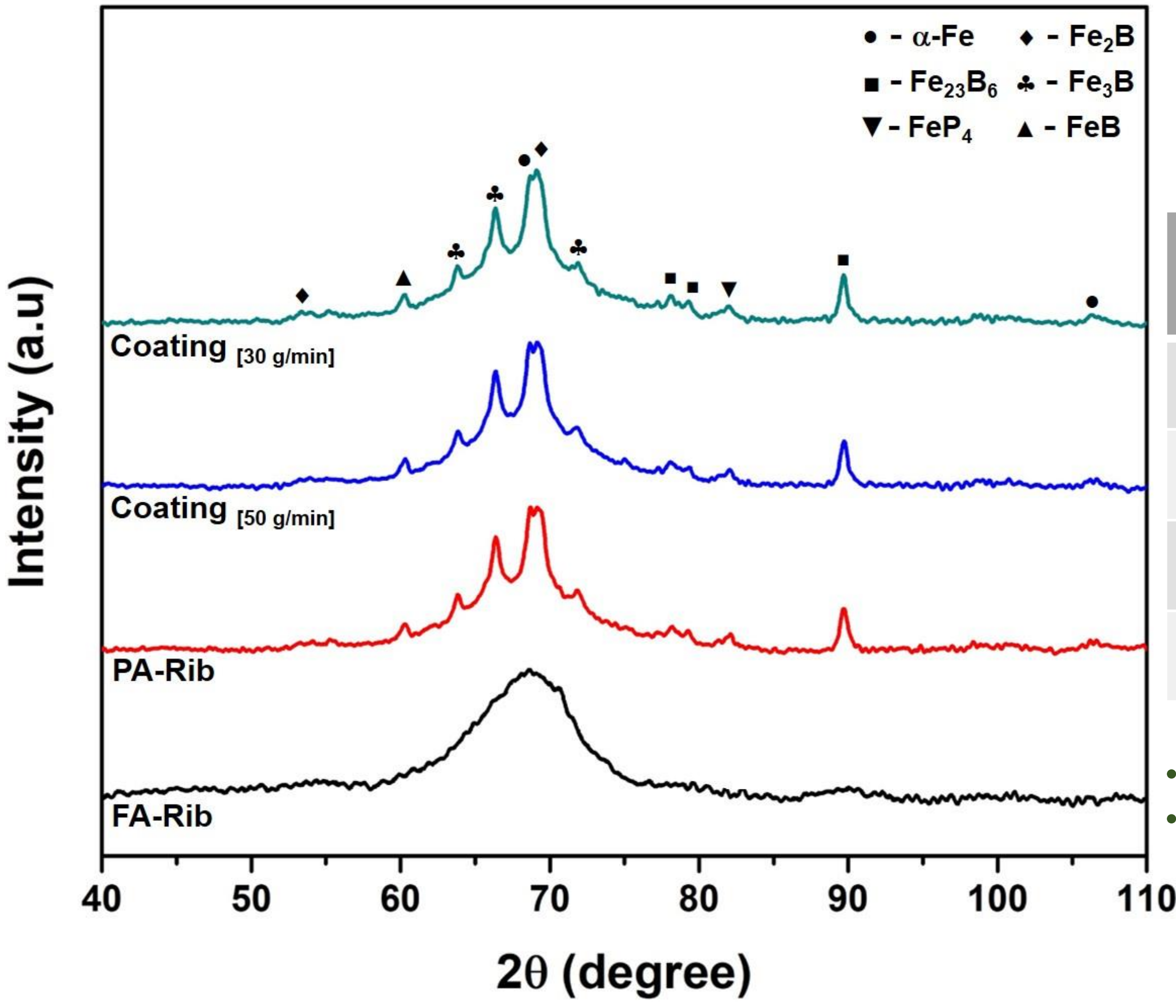

XRD patterns of FA-Rib, PA-Rib and the coatings

$$V_{amor} = \frac{A_{amor}}{A_{amor} + A_{Cryst}}$$

Sample	Amorphous content (%)
FA-Rib	100
PA-Rib	66
Coating [30 g/min]	65
Coating [50 g/min]	63

- **FA-Rib→ fully amorphous nature**
- **Amorphous content was almost same for PA-Rib, Coating [50 g/min] and Coating [30 g/min]**

S.K. Nayak et al., J. Alloys Compd. 849 (2020) 156624

RESULTS

Phase evolution in the ribbons and the coatings

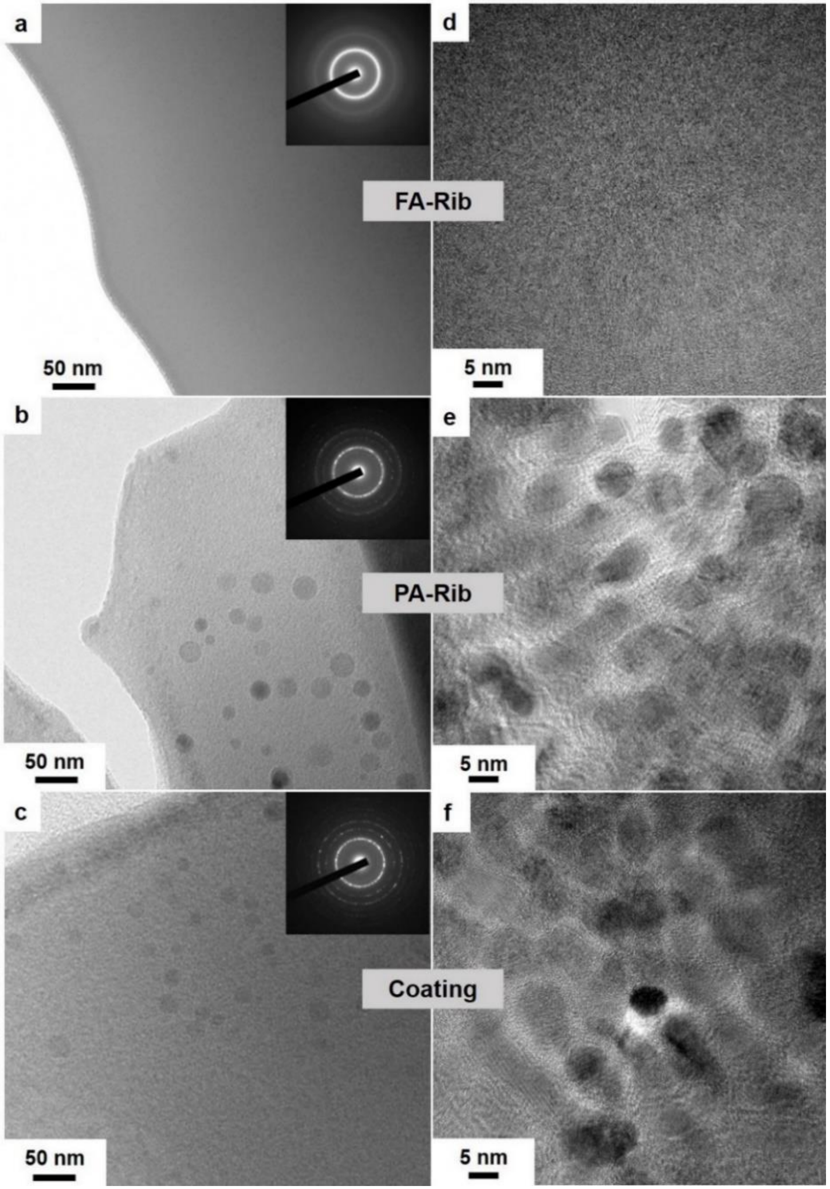

- FA-Rib→ fully amorphous structure is confirmed
- Nanocrystalline phases dispersed in the amorphous matrix of PA-Rib and Coating $_{[50\ g/min]}$

TEM images of (a) FA-Rib, (b) PA-Rib and (c) Coating $_{[50\ g/min]}$ with corresponding SAED patterns in insets depicting variation in amorphicity, and HRTEM micrographs of (d) FA-Rib, (e) PA-Rib and (f) the coating

S.K. Nayak et al., J. Alloys Compd. 849 (2020) 156624

RESULTS

Corrosion behavior: Potentiodynamic Polarization

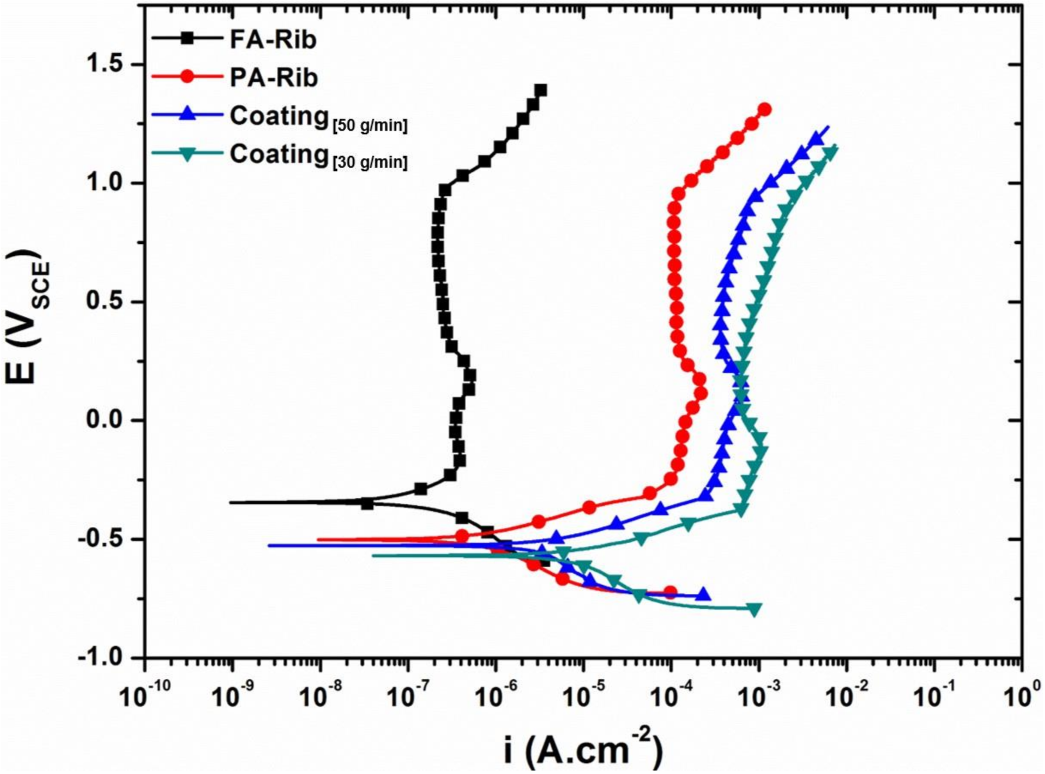

Potentiodynamic polarization curves of the different ribbons and the coatings in 3.5 wt. % NaCl solution

- **Corrosion of the amorphous matrix increased substantially due to its partial crystallization compared to porosity effect.**

Sample	E_{corr} (mV)	i_{corr} (μA.cm^{-2})	i_{pass} (μA.cm^{-2})	E_{pit} (mV)
FA-Rib	-344 ± 4	0.09 ± 0.01	0.26 ± 0.09	982 ± 4
PA-Rib	-501 ± 5	0.62 ± 0.10	114.7 ± 8.6	937 ± 6
Coating [50 g/min]	-524 ± 7	3.2 ± 0.4	386.5 ± 7.3	923 ± 5
Coating [30 g/min]	-567 ± 8	8.3 ± 0.6	873.4 ± 9.7	908 ± 9

S.K. Nayak et al., J. Alloys Compd. 849 (2020) 156624

Corrosion behavior: Electrochemical Impedance Spectroscopy

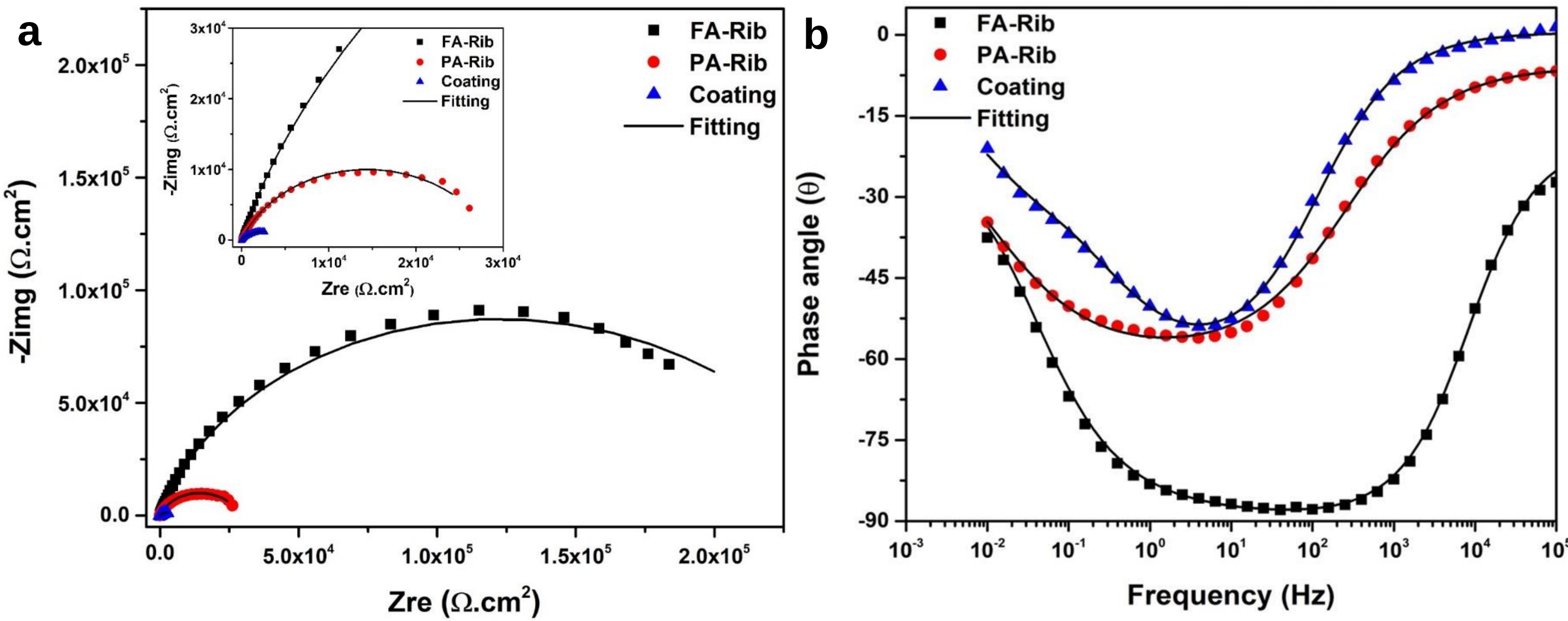

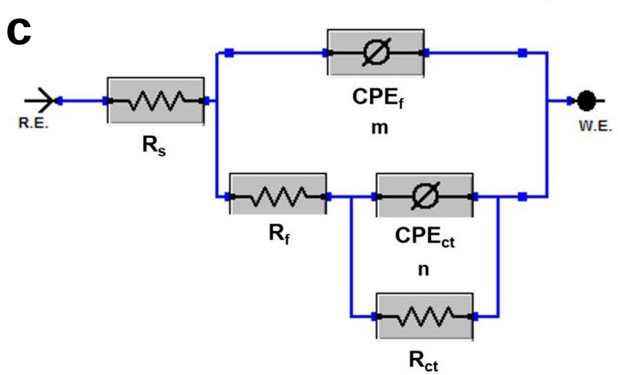

Electrochemical impedance plots of the samples at OCP: (a) Nyquist plot (b) Bode phase angle plot and (c) electrical equivalent circuit

Sample	R_f (kΩ.cm²)	R_{ct} (kΩ.cm²)	R_t (kΩ.cm²)	GOF ($x10^{-4}$)
FA-Rib	16.2	246	262.2 ↓	5.5
PA-Rib	2.9	27.5	30.4 ↓	3.2
Coating [50 g/min]	1.6	3.3	4.9	2.3

S.K. Nayak et al., J. Alloys Compd. 849 (2020) 156624

RESULTS

Corroded surface analysis

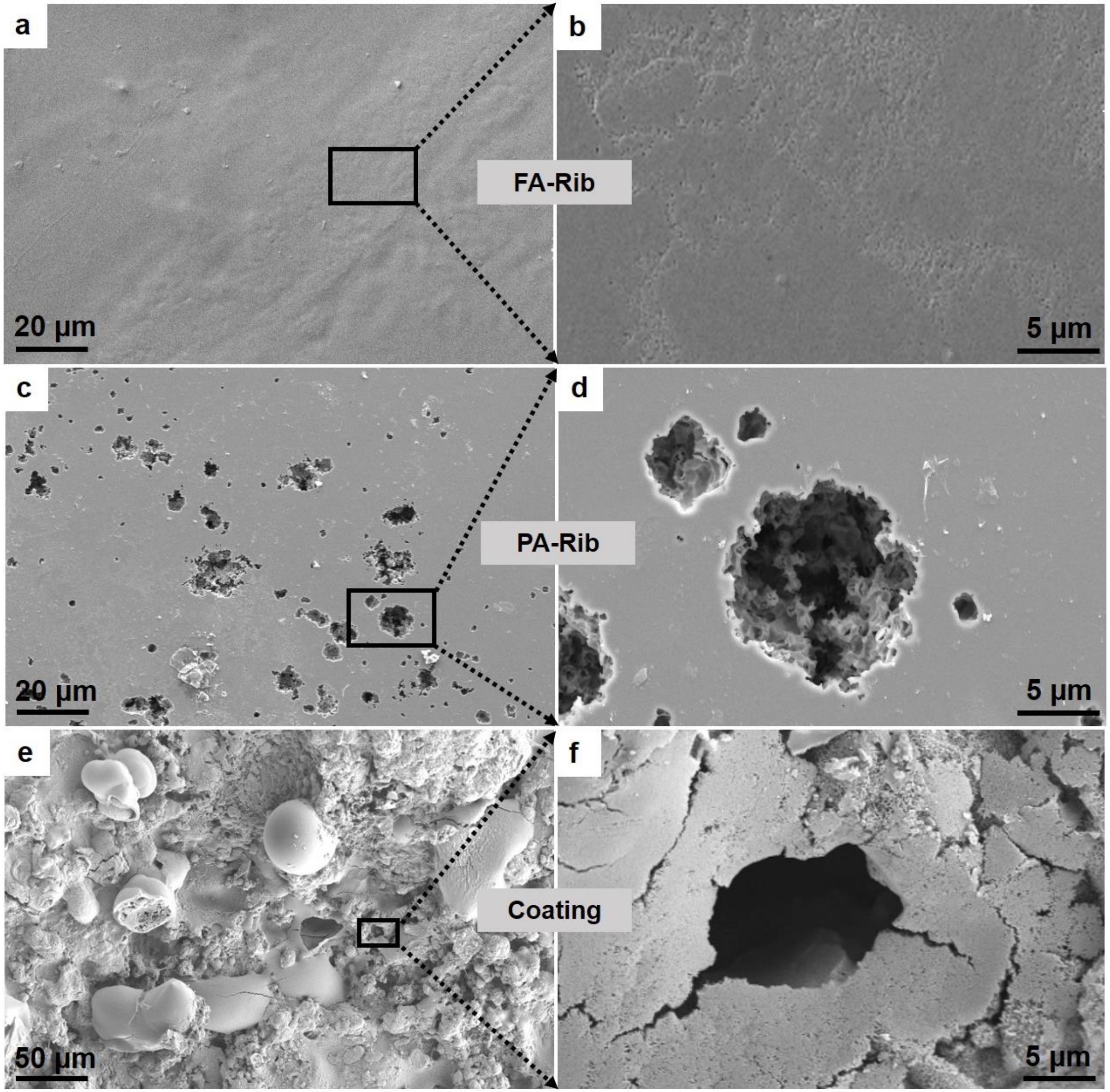

- **FA-Rib→ pits in the nano-scale range at higher magnification**
- **PA-Rib→ uniformly distributed pits in the size range of 1-10 µm**
- **Coating→ selective dissolution, very large (>10 µm) and deep pits**

SEM micrographs of the corroded surface: (a–b) FA-Rib, (c–d) PA-Rib and (e–f) the coating

S.K. Nayak et al., J. Alloys Compd. 849 (2020) 156624

Analysis of corrosion products

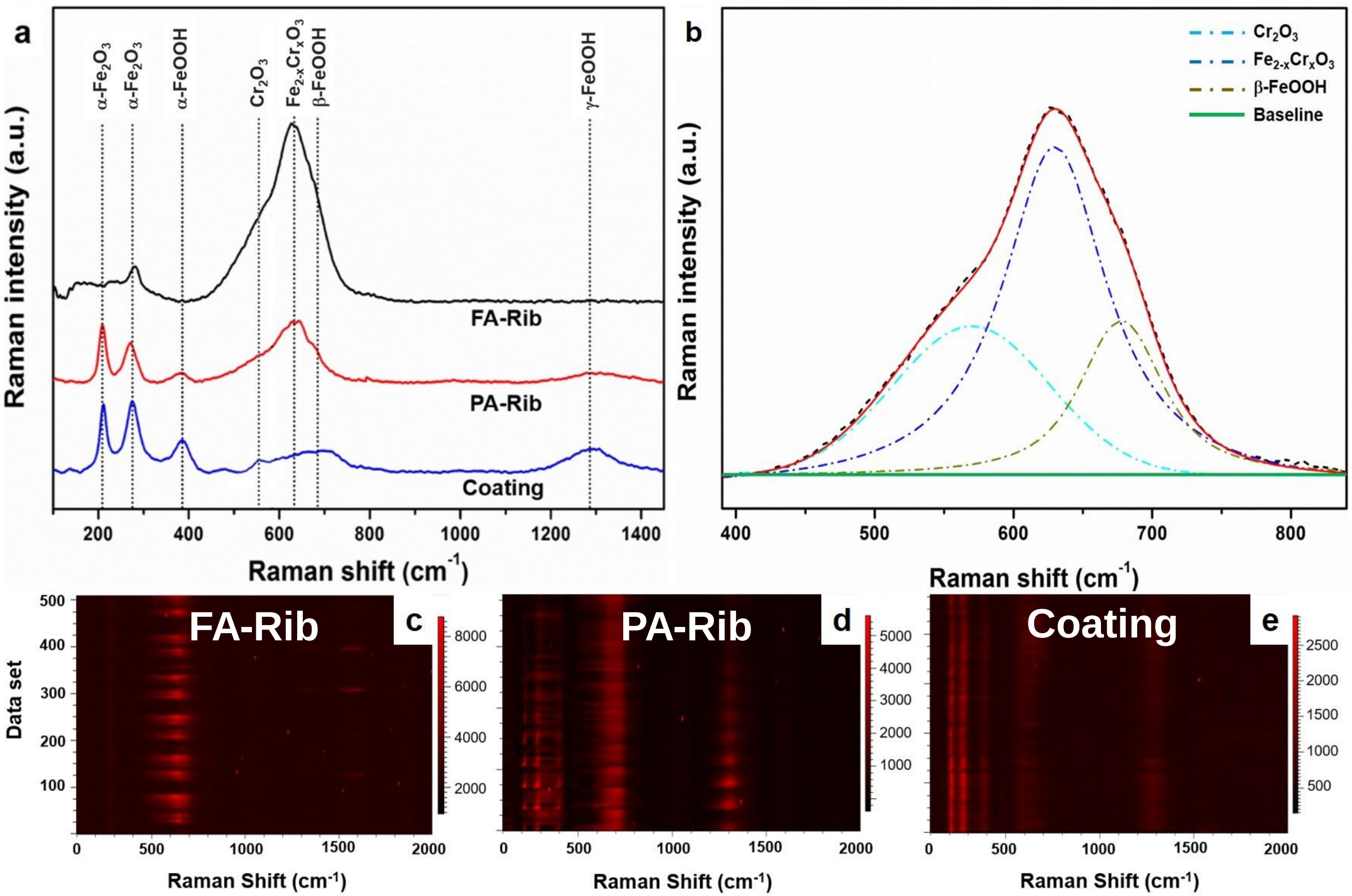

a) Raman spectra of the post-polarized ribbons and coating, (b) de-convoluted Raman spectrum of FA-Rib and (c–e) Raman spectra intensity distribution of the various products

- **Relative fraction of protective phases (Cr_2O_3 and $Fe_{2-x}Cr_xO_3$):** ***FA-Rib (0.79), PA-Rib (0.38) and the coating (0.21)***
- **Greater influence of reduced amorphicity than that of porosity on the formation of protective phases**

S.K. Nayak et al., J. Alloys Compd. 849 (2020) 156624

RESULTS

Passive film analysis

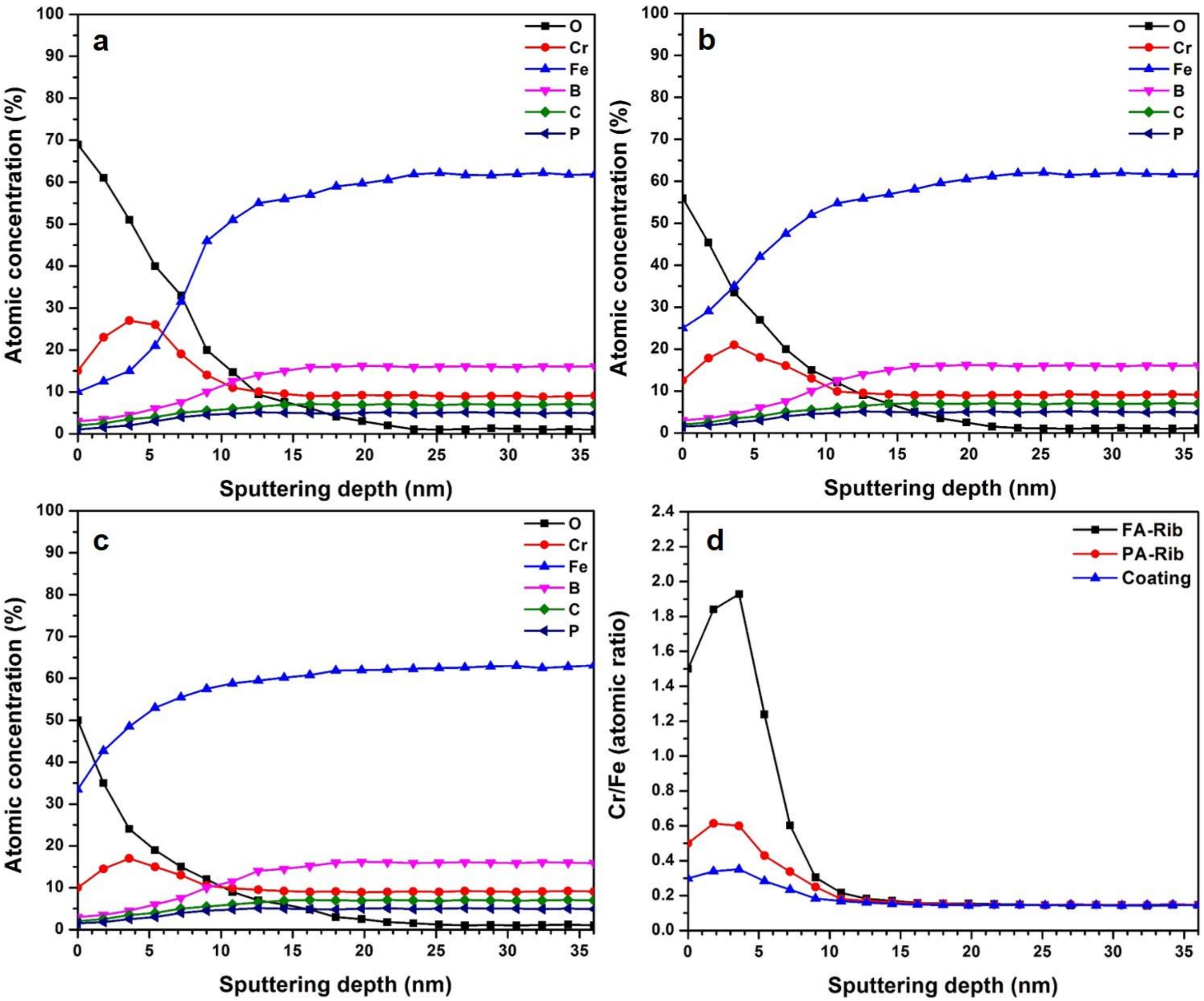

- **Thickness of the passive film:**
  (i) FA-Rib (~7.1 nm)
  (ii) PA-Rib (~4.8 nm)
  (iii) the coating (~3.7 nm)
- **Maximum value of Cr/Fe:**
  (i) FA-Rib- ~1.9
  (ii) PA-Rib- ~0.6
  (iii) the coating- ~0.3
- **Thinning as well as depletion of Cr in the passive film→ majorly by amorphicity**

AES concentration depth profiles of various elements obtained from passive films formed on the surface of (a) FA-Rib, (b) PA-Rib and (c) the coating and (d) Cr/Fe ratio in passive films of the samples

S.K. Nayak et al., J. Alloys Compd. 849 (2020) 156624

Correlation between corrosion behavior and microstructural features

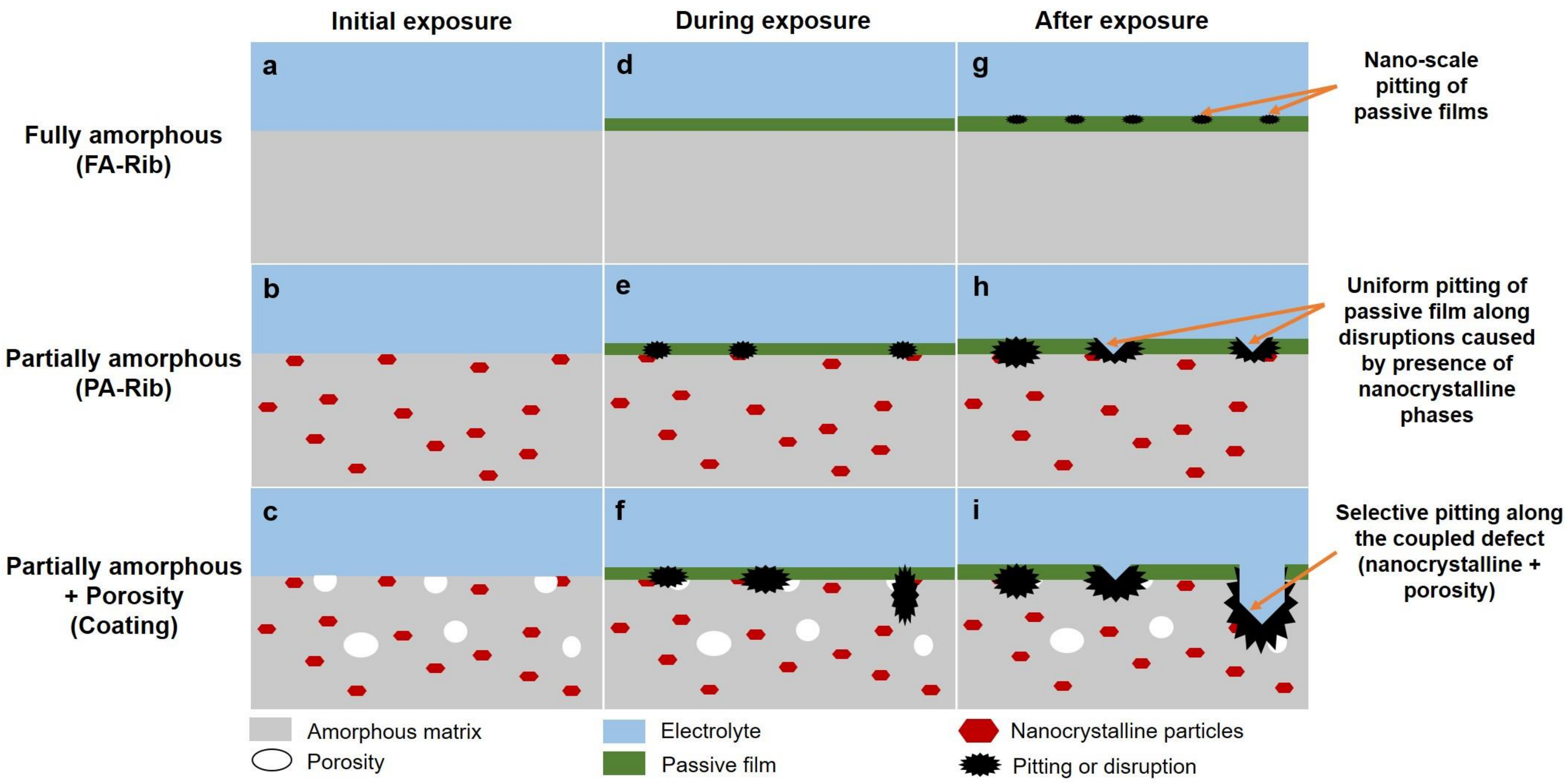

Schematic illustration of the corrosion process during different periods of immersion in electrolyte

S.K. Nayak et al., J. Alloys Compd. 849 (2020) 156624

CONCLUSION

Morphology of corroded surface

Extent of pitting (↑)

Electrochemical Impedance Spectroscopy

1. R_t (↓)
2. Phase angle maxima (↓)

Composition of corrosion products

Fraction of protective phases (↓)

Dominant effect of reduced amorphicity over porosity on corrosion behavior of Fe-based amorphous composite coatings

Potentiodynamic polarization study

1. i_{corr}(↑) and i_{pass}(↑)
2. E_{corr}(↓) and E_{pit}(↓)

Passive film analysis

1. Thinning (↑)
2. Hindrance to Cr enrichment (↑)

* (↑) – Increase (↓) – Decrease

Publications related to this work

- **S.K. Nayak**, A. Kumar, K. Sarkar, A. Banerjee and T. Laha, Mechanistic insight into the role of amorphicity and porosity on determining the corrosion mitigation behavior of Fe-based amorphous/nanocrystalline coating, *Journal of Alloys and Compounds* 849 (2020) 156624.
- **S.K. Nayak**, A. Kumar, K. Sarkar, A. Pathak, A. Banerjee and T. Laha, A study on the corrosion inhibition of Fe-based amorphous/nanocrystalline coating synthesized by high-velocity oxy-fuel spraying in an extreme environment, *Journal of Thermal Spray Technology* 28 (2019) 1433-1447.
- A. Kumar, **S.K. Nayak**, K. Sarkar, A. Banerjee, K. Mondal and T. Laha, Investigation of nano-and micro-scale structural evolution and resulting corrosion resistance in plasma sprayed Fe-based (Fe-Cr-B-C-P) amorphous coatings, *Surface and Coatings Technology* 397 (2020) 126058.
- P. Bijalwan, A. Kumar, **S.K. Nayak**, A. Banerjee, M. Dutta and T. Laha, Microstructure and corrosion behavior of Fe-based amorphous composite coatings developed by atmospheric plasma spraying, *Journal of Alloys and Compounds* 796 (2019) 47-54.


Thank You
For Your Attention